Molecular Biology of the Cell
Vol. 15, 5603–5615, December 2004

Bipolarization and Poleward Flux Correlate during *Xenopus* Extract Spindle Assembly[V]

T.J. Mitchison,*†‡§ P. Maddox,*‡‖ A. Groen,*†‡ L. Cameron,*‡‖ Z. Perlman,*† R. Ohi,*† A. Desai,*¶ E.D. Salmon,*‖ and T.M. Kapoor*#

*Cell Division Group, Marine Biological Laboratory, Woods Hole, MA 02543; †Department of Systems Biology, Harvard Medical School, Boston, MA 02115; ‖Department of Biology, University of North Carolina, Chapel Hill, NC 27599; ¶Rockefeller University, New York, NY 10021; and #Department of Cellular and Molecular Medicine, University of California at San Diego, La Jolla, CA 92093

Submitted May 31, 2004; Revised September 2, 2004; Accepted September 3, 2004
Monitoring Editor: Tim Stearns

We investigated the mechanism by which meiotic spindles become bipolar and the correlation between bipolarity and poleward flux, using *Xenopus* egg extracts. By speckle microscopy and computational alignment, we find that monopolar sperm asters do not show evidence for flux, partially contradicting previous work. We account for the discrepancy by describing spontaneous bipolarization of sperm asters that was missed previously. During spontaneous bipolarization, onset of flux correlated with onset of bipolarity, implying that antiparallel microtubule organization may be required for flux. Using a probe for TPX2 in addition to tubulin, we describe two pathways that lead to spontaneous bipolarization, new pole assembly near chromatin, and pole splitting. By inhibiting the Ran pathway with excess importin-alpha, we establish a role for chromatin-derived, antiparallel overlap bundles in generating the sliding force for flux, and we examine these bundles by electron microscopy. Our results highlight the importance of two processes, chromatin-initiated microtubule nucleation, and sliding forces generated between antiparallel microtubules, in self-organization of spindle bipolarity and poleward flux.

INTRODUCTION

To segregate chromosomes, mitotic and meiotic spindle must be bipolar. Bipolarization is thought to occur by one of two pathways (reviewed in Karsenti and Nedelec, 2004). In the microtubule organizing center (MTOC) driven pathway, the MTOC duplicates, the resulting pair separates, and a bipolar spindle assembles between the paired MTOCs, driven in part by selective stabilization of microtubules making correct interactions (Kirschner and Mitchison, 1986). This pathway is thought to dominate in many embryonic mitotic spindles and also in fungal mitotic and meiotic spindles. In the self-assembly, or spontaneous bipolarity pathway, microtubules are nucleated near chromatin, and then they self-organize into a bipolar array (Karsenti and Vernos, 2001). Self-organization of bipolarity is thought to involve cooperative action of plus end– and minus end–directed motor protein complexes with the capacity to exert forces between microtubules (Walczak *et al.,* 1998; Nedelec, 2002). This pathway dominates in spindles that lack a defined MTOC, such as oocyte meiotic spindles in insects and vertebrates and probably also in higher plant mitotic spindles (Matthies *et al.,* 1996; Smirnova and Bajer, 1998). The two pathways for achieving bipolarity are not mutually exclusive. For example, ablation (Khodjakov *et al.,* 2000) or displacement (Rebollo *et al.,* 2004) of MTOCs revealed the presence of the spontaneous pathway in normal centrosome-dominated systems. This apparent redundancy may make achievement of bipolarity robust to mistakes or perturbation.

Much remains to be learned about the spontaneous bipolarization pathway. Most research in this area has focused on the role of motor proteins (e.g., Matthies *et al.,* 1996; Walczak *et al.,* 1998; Nedelec, 2002). The role of microtubule polymerization dynamics in bipolarization has not been addressed in detail, and the intermediate organizational states explored on the pathway to bipolarity have not been well described. In this article we explore bipolarization using *Xenopus* egg extracts. Unfertilized *Xenopus* eggs are arrested in metaphase of meiosis II, and spindles assembled in egg extract recapitulate egg meiosis II spindle morphology and size (Sawin and Mitchison, 1991a). In the egg, *Xenopus* meiosis occurs without centrosomes, and extract spindles are thought to achieve bipolarity using primarily the spontaneous pathway (Heald *et al.,* 1996; Walczak *et al.,* 1998). Centrosomes catalyze spindle pole assembly in egg extracts if they are present (Heald *et al.,* 1997), as in this study and other standard experiments using permeabilized *Xenopus* sperm nuclei as a source of chromatin (Desai *et al.*, 1999a).

One of the more remarkable dynamic behaviors of bipolar mitotic and meiotic spindles at metaphase is continuous poleward sliding of microtubules while the spindle maintains a steady state in length. This behavior, termed poleward flux, has been observed or inferred in mitotic and meiotic spindles in several cell types, as well as *Xenopus* extracts (Mitchison and Sawin, 1990; Sawin and Mitchison, 1991b; Brust-Mascher and Scholey, 2002; Maddox *et al.,*

Article published online ahead of print. Mol. Biol. Cell 10.1091/mbc.E04–05–0440. Article and publication date are available at www.molbiolcell.org/cgi/doi/10.1091/mbc.E04–05–0440.

[V] The online version of this article contains supplemental material at MBC Online (http://www.molbiolcell.org).

‡ These authors contributed equally to this work.

§ Corresponding author. E-mail address: timothy_mitchison@hms.harvard.edu.

2002), but probably not in yeast (Mallavarapu *et al.*, 1999; Maddox *et al.*, 2000). It therefore seems to be a widely conserved process in large spindles, but not a fundamental requirement for bipolarity or chromosome segregation. The functions of flux, and the molecular mechanisms that drive it, are incompletely understood, but it seems likely that flux itself, or some of the molecular mechanisms underlying flux, might play an important role in spindle assembly and achievement of bipolarity. At a molecular level, flux is thought to require three coordinated activities: polymerization, sliding of the microtubule lattice toward the pole, and depolymerization. Polymerization is thought to occur only on plus ends, both kinetochore-attached and free (Mitchison *et al.*, 1986). Polymerization requires continuous nucleation of microtubules to balance those lost by dynamic instability. Nucleation can occur both at poles and near chromosomes (Karsenti and Nedelec, 2004), but the relative contribution of these sites in different types of spindle has not been measured. Recent work using small molecule inhibitors and immunodepletion/add-back suggested that he sliding component of poleward flux in *Xenopus* extract metaphase spindles is driven primarily by the kinesin Eg5 (Miyamoto *et al.*, 2004). Depolymerization associated with flux can occur on both ends of microtubules. Nonkinetochore spindle microtubules undergo rapid dynamic instability, which promotes fast depolymerization from plus ends throughout the spindle (Sawin and Mitchison, 1991b). Subunit loss from minus ends, if it occurs in these microtubules, would only account for a small faction of turnover. The plus ends of kinetochore microtubules are stabilized against rapid depolymerization, and flux in these microtubules is thought to require depolymerization of minus end at poles, probably driven by an active destabilizing activity, such as a KinI kinesin (Rogers *et al.*, 2004). With recent observations implicating specific molecules in subreactions of flux (Eg5 in sliding, KinI kinesins in minus end depolymerization), we may be closing in on the molecular mechanism of flux, but important questions remain. In particular we do not understand the organizational requirements for flux or how the subreactions are coordinated to achieve a steady state in spindle length.

An appealing model for flux proposes that the sliding component is driven by the action of plus end–directed molecular motors that directly cross-bridge antiparallel microtubules (reviewed in Mitchison and Sawin, 1990; Sharp *et al.*, 2000). The bipolar structure of Eg5 suggests it might push antiparallel overlapping microtubules apart (Kashina *et al.*, 1996), and recent work implicated this kinesin in generating the sliding force for flux (Miyamoto *et al.*, 2004). This model predicts a requirement for bipolar spindle organization to generate flux, but experiments in *Xenopus* extracts were interpreted as demonstrating flux in monopolar microtubule asters (Sawin and Mitchison, 1994). However, those experiments used an intensifying camera with imaging characteristics that were poor by current standards. Here we reinvestigate flux in monopolar asters and find that they do not flux, removing an objection to the antiparallel cross-bridge motor model. We also describe the pathways that drive spontaneous bipolarization in detail and the consequence of removing antiparallel microtubules by inhibiting the Ran pathway.

MATERIALS AND METHODS

CSF extracts and cycled spindles were made by standard methods (Desai *et al.*, 1999a). Setups for widefield and confocal spinning disk fluorescence speckle microscopy have been described elsewhere (Desai *et al.*, 1999a; Maddox *et al.*, 2003). Optimal concentrations of X-rhodamine tubulin for confocal speckle imaging were determined empirically for each extract, with ~50 nM typical. affinity-purified antibodies to C-terminal peptides of TPX2 ((C)VKASDVPLTVPRSPNFSDRFKA; Research Genetics, Huntsville, AL) and NUMA ((C)TAKSPRASNKLFERKQQRNK; Research Genetics) were made as described (Field *et al.*, 1998), using cysteine coupling alone. Both antibodies were specific on Western blots, gave the reported localization patterns in fixed spindles, and did not perturb spindle assembly or microtubule dynamics at tested concentrations (up to 10 μg/ml). Alexa 488-IgG conjugates were prepared as suggested by the manufacturer (Molecular Probes, Eugene, OR) and dialyzed into 10 mM K-HEPES (pH 7.7), 100 mM KCl for use in *Xenopus* egg extracts. The CenpA IgG probe was made similarly (Maddox *et al.*, 2003). Fluorescent probes were added either before second CSF addition or after spindle assembly, at final concentrations of 0.5–5 μg/ml. We empirically determine the minimal probe concentrations necessary to image each protein and checked that there was no change in spindle morphology and flux rate by comparison to samples without probes and previous data. His-tagged *Xenopus* importin-alpha (clone kindly provided by K. Weis, U. CA Berkeley) was expressed in *Escherichia coli* and purified using Ni^{2+} chromatography as described (Gorlich *et al.*, 1994), with an added gel filtration step in 10 mM K-HEPES (pH 7.7), 200 mM KCl, 1 mM DTT to remove truncated fragments. It was >90% pure by SDS-PAGE, and was stored frozen in small aliquots. Flow chambers were made with two thin strips of double-stick tape placed a few millimeters apart between a coverslip and slide. They were filled with 5–10 μl of extract containing CSF monopoles, and sealed with valap (1:1:1 vasoline:lanolin:parafin). For confocal imaging of cycled spindles and widefield imaging of monopoles, 2–6 μl of extract was spread under a 18-mm^2 coverslip and sealed with valap. Electron microscopy of cycled spindles was performed as described (Ohi *et al.*, 2003).

Sequential images were aligned to compensate for rotation and translation using a homemade MATLAB program (The Mathworks, Natick, MA) called ALIGNER that automatically performed the following operations. In an optional step, the image sequence was first blurred to remove detailed speckle information. This results in alignment based on low spatial frequencies. It was used in aligning speckle images to prevent possible speckle flow within the structure, or bright pixels, from dominating the alignment. Sequential images in the sequence were rotated to a series of positions ($\theta = 0; \pm 0.5, 1, 2, 4^{\circ}$) using subpixel sampling and cubic interpolation to generate the rotated image. For each rotation, cross correlation with the previous image was calculated for all x,y translations using the formula. The maximum cross-correlation value was plotted against θ, and fit to a quadratic curve. The peak of this curve was calculated to generate the x, y, θ values that maximize cross-correlation between sequential images. These values were applied to the image, and all subsequent images in the sequence, as the alignment procedure moved through the time series. Finally the calculated optimal x, y, θ values were applied back to the original, unblurred image sequence. ALIGNER plus documentation is available from Zach Perlman. Kymographs were generated using METAMORPH software (Universal Imaging, West Chester, PA).

RESULTS

Monopolar Asters Do Not Flux

We set out to readdress the question of whether monopolar sperm asters (CSF monopoles) exhibit poleward flux using confocal speckle imaging. CSF monopoles were made by adding sperm to mitotic extract and fixing or initiating time-lapse imaging within 30 min. CSF monopoles typically have loosely focused poles and an asymmetric microtubule distribution, with most microtubules oriented from the pole toward chromatin (Figure 1A). Bipolar spindles were made either by allowing CSF monopoles to become bipolar by further incubation in mitotic extract to make CSF bipolar spindles (Figure 1B), or by replicating sperm DNA in interphase extract and then adding back CSF extract to assemble spindles that are capable of chromosome segregation ("cycled spindles"). These manipulations were described previously, and bipolarization of CSF monopoles in solution was attributed to pair-wise fusion (Sawin and Mitchison, 1991a). To measure flux we imaged rhodamine-labeled tubulin at speckle levels by spinning disk confocal microscopy (Maddox *et al.*, 2003). Two additional technical innovations were important. For live imaging of CSF monopoles we used flow chambers made with double-stick tape. The extract layer is ~70-μm thick in these squashes, which reduces interaction between microtubules and the glass surface compared with the more typical thin (8–16 μm) squashes of extract between slide and coverslip used previously. We also developed a

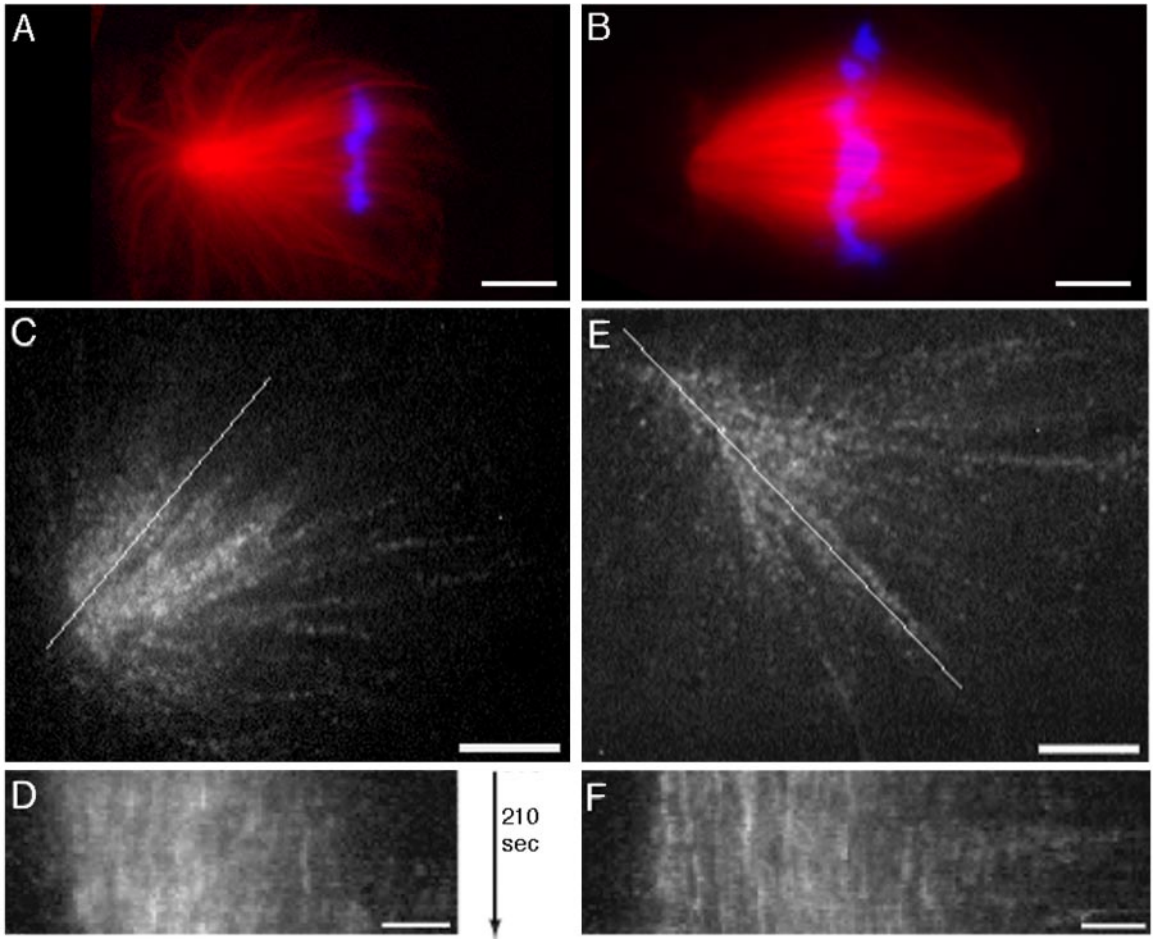

Figure 1. CSF monopoles do not show evidence of flux by tubulin speckle microscopy. (A and B) Examples of fixed CSF monopoles and bipoles for reference. (C and E) Examples of CSF monopoles labeled with rhodamine tubulin at speckle levels that were followed by confocal microscopy, aligned, and kymographed. Two examples are shown from the 12 examples out of 20 sequences collected where the structure remained monopolar throughout the sequence. (A) Example of a typical CSF monopoles imaged by fixation 25 min after addition of sperm to CSF extract. Red signal is rhodamine tubulin, and blue is DNA. Note the asymmetric distribution of microtubules toward chromatin. Bar, 10 μm. (B) Example of a typical bipolar spindles formed by further incubation of the reaction shown in A. Fixation at 70 min after addition of sperm nuclei. Note that chromatin-pole distance is similar in bipoles and CSF monopoles. Bar, 10 μm. (C) Example of a CSF monopole by confocal imaging of tubulin at speckle levels. The chromatin is toward the right. The line was used to generate the kymograph in D. Bar, 5 μm. See Supplementary Video M1_1 (before alignment) and M1_2 (after alignment). (D) Kymograph of the monopole in C. Note the mostly vertical streaks, indicating no sliding of microtubules within the structure. Bar, 2 μm. (E) Another example of a CSF monopole by speckle imaging of tubulin. The line was used to generate the kymograph in F. Bar, 5 μm. See Supplementary Video M1_3 (after alignment). (F) Kymograph of the monopole in E. Bar, 2 μm.

method for computationally aligning a moving object between sequential images that compensates for translation and rotation, facilitating detection of flux. Our alignment program is based on maximizing cross-correlation between sequential images and may be useful for other applications.

When observed in flow chambers, asymmetric CSF monopoles typically moved across the field with the chromatin side leading, perhaps driven by cytoplasmic dynein. Movement rate was variable, with frequent pauses. We measured a mean rate of 7 μm/min (range 2–13 μm/min, n = 7; Supplementary Video M1_1). This movement made analysis of speckle flow difficult, so we developed a computational alignment procedure to reposition the aster in sequential frames, rendering it approximately static (compare Supplementary Videos M1_1 and M1_2). We then assayed flow of speckles, indicative of microtubule sliding within the monopole, by visual inspection and kymography of the aligned sequences. Two examples are shown in Figure 1, C–F, and Supplementary Videos M1_2 and M1_3. By visual inspection, speckles continuously appear and disappear due to microtubule turnover, but there is no evidence for concerted movement of speckles within the monopoles. Kymographs through the aligned CSF monopoles showed mostly vertical steaks, indicating mostly static speckles (Figure 1, D and F). In some cases we did observe individual kymograph streaks moving toward or away from the poles, suggesting limited, concerted movement in subregions of CSF monopoles (e.g., Figure 2B2). We interpret these as indicating condensation and reorganization of the pole. We did not observe concerted movement of speckles toward poles in kymographs of CSF monopoles, the hallmark of flux in bipolar spindles. In contrast, both CSF and cycled bipolar spindles always showed concerted movement of speckles toward poles in supplementary videos and kymographs using the same methods (Maddox *et al.*, 2003; examples in Figure 3).

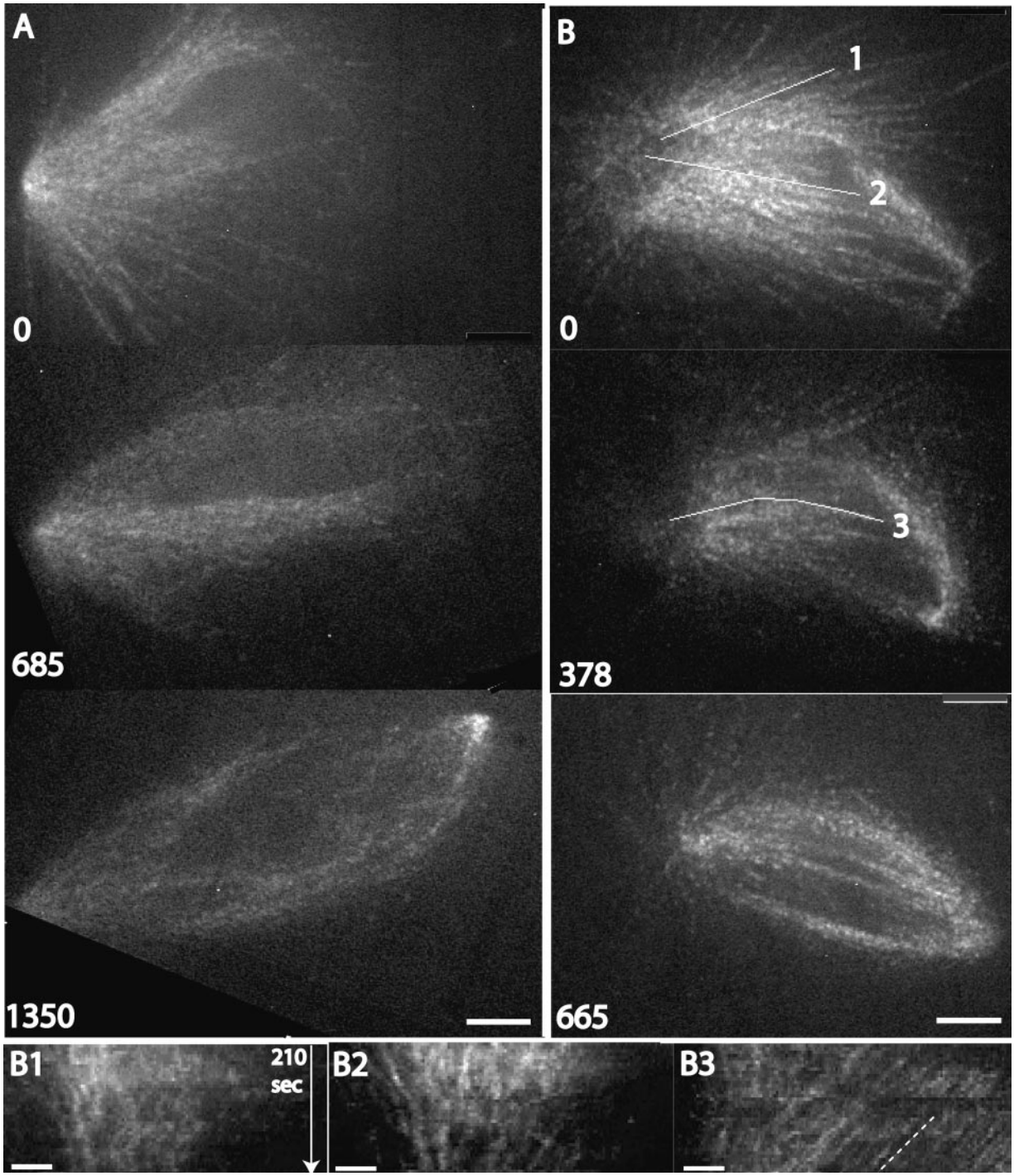

Figure 2. Spontaneous bipolarization of CSF monopoles, and initiation of flux. CSF monopoles labeled with rhodamine tubulin at speckle levels were followed by confocal microscopy, followed by image alignment to correct for movement of the structure. Two examples are shown from the 8 examples out of 20 sequences collected where bipolarization occurred in a flow chamber. (A) Example where the spindle structure was tracked during its evolution from a monopole to a symmetrical bipole. The speckle contrast is too low for kymography, but in the supplementary video evidence for bidirectional microtubule sliding can be seen after bipolarization. Elapsed time shown in seconds. Bar, 5 μm. See Supplementary Video M2_1. (B) Example with better speckle contrast. The first pole is to the left. At the first time point the structure already showed evidence of new pole formation to the right, but was still mainly monopolar. Later the structure evolved into a symmetrical bipole. The lines show where kymographs were collected. In the supplementary video, the structure shows little or no microtubule sliding early and robust bidirectional sliding late. Elapsed time shown in seconds. Bar, 5 μm. See Supplementary Video M2_2. (B1 and B2) Kymographs early in the sequence shown in B, starting at $t = 0$, along the lines indicated as 1 and 2. Bar, 2 μm. Early in the sequence (toward the top of kymograph) individual tubulin speckles are either static (vertical streaks) or moving slowly in an incoherent manner. There is some movement of speckles near the pole into the structure, which we think indicates the pole becoming more focused. (B3) Kymograph later in the sequence shown in B, starting at $t = 378$ s, along the line indicated as 3. By this time the structure showed coherent movement of speckles toward the old (left) pole in the supplementary video. Note the parallel, diagonal streaks in the kymograph, indicative of coherent microtubule sliding. The line is drawn parallel to these steaks to highlight them. Time axis as B1. Bar, 2 μm

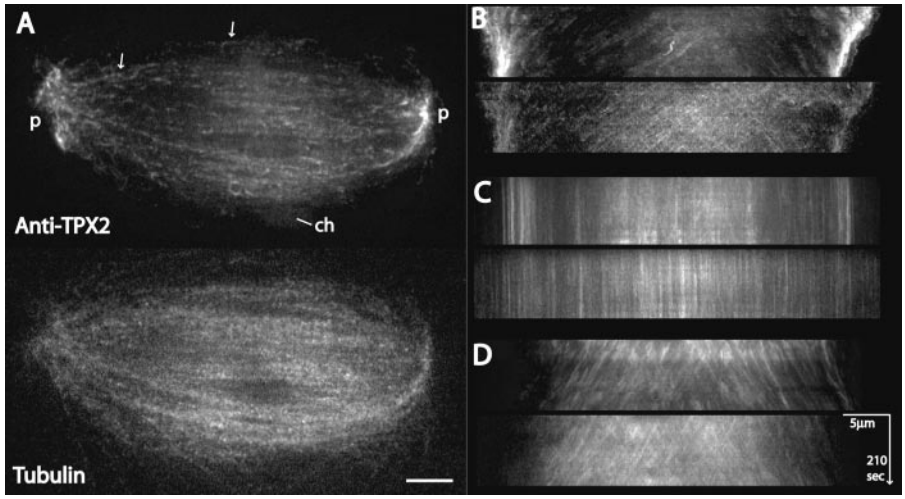

Figure 3. Labeled anti-TPX2 as a probe for spindle poles and flux. Cycled bipolar spindles were labeled with Alexa 488 anti-TPX2 (top panels in each pair) and rhodamine tubulin at speckle levels (bottom panels in each pair). All kymographs were taken on a line through both poles, with the time and scale bar shown in D. (A) Example of a bipolar spindle. The anti-TPX2 probe accumulates at the poles (p). It also labels puncta and fibrils throughout the spindle, which are partly coaligned with tubulin (e.g., arrows). Faint accumulation of the probe on chromatin can also been seen in this example (ch)aa. Bar, 5 μm. See Supplementary Video M3_1. (B) Kymograph of the spindle shown in A. Top panel, anti-TPX2; bottom panel, tubulin. Anti-TPX2 puncta and tubulin speckles move continuously toward the poles at the same rate, indicated by the diagonal steaks. This is diagnostic of poleward flux. Time and scale bar for B–D shown in D. See Supplementary Video M3_1. (C) Kymograph of a spindle treated with 2 mM AMPPNP. This treatment blocks poleward flux (Sawin and Mitchison, 1991b). Note that both anti-TPX2 puncta and tubulin speckles are static, indicated by vertical lines. In the supplementary video, the anti-TPX2 signal is much more tightly coaligned with tubulin in AMPPNP compared with control. See Supplementary Video M3_2. (D) Kymograph of a spindle assembled in the presence of p50 dynamitin (0.9 mg/ml), a dynactin antagonist that blocks pole assembly but not flux. Note poleward movement of anti-TPX2 puncta and tubulin speckles at the same rate. Note also that anti-TPX2 does not accumulate at the unfocussed poles. The rate of flux is slower in this example than B, but this was not always the case for p50 spindles. We are currently developing better tools to measure flux rate and explore its variability. See Supplementary Video M3_3.

Our failure to observe flux in CSF monopoles by imaging tubulin speckles partially contradicts a previous study that reported flux in a fraction of CSF monopoles using photoactivation of fluorescence (Sawin and Mitchison, 1994). To confirm our new, negative result, we collected sequential images from 20 CSF monopoles in flow chambers, following each for up to 20 min. We then divided them into 12 sequences where the aster remained truly monopolar and 8 sequences where it showed evidence of becoming bipolar (discussed below). We computationally aligned the monopolar sequences and analyzed them by eye and kymography. In no case did we see evidence for coherent movement of large numbers of speckles toward the pole, which would indicate the presence of flux. Because spontaneous bipolarization can be ambiguous in some sequences, we cannot guarantee that this statistic for flux in monopolar asters (0/12) is free of observer bias. However, when combined with observations made during bipolarization (discussed below), we feel confident that truly monopolar CSF sperm asters in *Xenopus* extracts do not display concerted microtubule flux either toward or away from poles, at least at the detection limit of current speckle imaging technology.

Spontaneous Bipolarization and Initiation of Flux

When we tracked CSF monopoles for >10 min, 8 of 20 underwent a spontaneous transition from monopolar to bipolar (Figure 2A, Supplementary Video M2_1). When CSF monopoles started to bipolarize, they also started to show evidence of coherent microtubule sliding within the structure that is typical of poleward flux in bipoles. Initiation of sliding is evident in Supplementary Video M2_1, but the speckle contrast in this long sequence was too low for kymograpy. Figure 2B (Supplementary Video M2_2) shows an example of a spindle that had just begun to assemble a second pole when the sequence was started and goes on to become obviously bipolar. Visual inspection, and kymographs, indicate that there was no coherent movement of speckles toward the first (left) pole early in the sequence, evident from the lack of parallel, diagonal streaks in the early kymograph (Figure 2, B1 and B2). The first pole becomes compressed early in the sequence, which was typical of monopoles undergoing bipolarization, and this leads to some pole-associated speckles moving toward the chromatin. This kind of limited microtubule sliding with a subregion is likely to be mechanistically different from the sliding associated with true flux, which tends to be coherent, and involve most or all of a half-spindle. Later, once the spindle was clearly bipolar, coherent movement of speckles toward the first pole started, evident from the parallel, diagonal streaks in the later kymograph (Figure 2B3). Because of movement, focal plane shifts, and photobleaching, we found it technically difficult to follow the full course of bipolarization while obtaining images of the quality necessary for speckle tracking. However, by visual inspection of eight sequences where bipolarization was followed live in flow chambers by imaging tubulin at speckle levels, we consistently observed a correlation between becoming bipolar and initiating coherent sliding of microtubules toward poles that is typical of flux.

We next set out to better understand the pathways by which single CSF monopoles become bipolar. To improve our ability to track pole assembly and movement we sought a marker for directly imaging poles. TPX2 is a microtubule associated protein that localizes predominantly to poles in *Xenopus* extract spindles and is an important component of the pathway from Ran activation to spindle assembly (Wittmann *et al.*, 2000; Gruss *et al.*, 2001). We made an affinity-purified antibody to the C-terminus of TPX2 that was specific on immunoblots and showed the reported localization of TPX2 by immunofluorescence in fixed spindles (unpublished data). We then labeled it with Alexa 488 as a live imaging probe. When we added the labeled antibody to extracts at a concentration of 1–5 μg/ml, together with sperm nuclei and rhodamine tubulin, it had no observable effect on assembly of CSF monopoles or bipolar spindles or on flux as measured by speckle microscopy in the tubulin

channel. When added to bipolar spindles, the anti-TPX probe accumulated at poles, providing a useful pole marker (p in Figure 3A). It also localized at lower levels to the body of the spindle, often in the form of puncta and thin strands or filaments that were not precisely coaligned with microtubules (arrows in Figure 3A). To a low and variable extent, it sometimes localized to chromatin in the center of the spindle (ch in Figure 3A), perhaps reflecting the site of GTP exchange on Ran, which leads to release of TPX2 from importin (Gruss *et al.*, 2001). Movies (Supplementary Video M3_1) and kymographs (Figure 3B) revealed that the puncta and thin strands of anti-TPX2 in the spindle body moved continuously poleward at the same rate as tubulin speckles (~2 μm/min; Figure 3B). Poleward movement of both markers was blocked by AMPPNP (Figure 3C, Supplementary Video M3_2), but not p50 dynamitin (Figure 3D, Supplementary Video M3_3). Thus poleward movement of the anti-TPX2 probe is presumably driven by attachment of TPX2 to fluxing microtubules. We conclude that our labeled anti-TPX2 antibody is a useful probe for pole assembly and flux. We do not assume it is a reliable probe for the details of TPX2 localization or dynamics—a directly labeled protein might be better for that—but our purpose in this article was only to follow poles and flux.

To image spontaneous bipolarization, sperm nucleii were added to CSF extract containing speckle levels of X-rhodamine tubulin, Alexa 488-anti-TPX2 IgG, and DAPI, and incubated for 10–20 min to allow formation of CSF monopoles. Samples were then observed in flow chambers by confocal microscopy (tubulin and anti-TPX2 only) or in thin squashes by widefield microscopy (all 3 probes). The thin squash conditions are more similar to those used previously (Sawin and Mitchison, 1994). Typically, the asters were initially asymmetric monopoles. Over the next 5–20 min, their morphology become more complex, in some cases leading to bipolar structures and in others to more complex, multipolar structures. Evidence for bipolarization was observed in ~40% of the flow chamber sequences experiments (8 of 20), and ~70% of the thin squash sequences (6 of 9). True bipolarization was observed in several of the flow chamber sequences (e.g., Figure 2), whereas the thin squashes more often gave rise to complex, multipolar assemblies.

Spontaneous bipolarization appeared to involve two processes, new pole assembly over chromatin, and pole splitting. Figure 4A (Supplementary Video M4_1) shows an example of bipolarization by pole assembly over chromatin. The chromatin was not directly imaged by two-color confocal microscopy, but its presence can be inferred in the microtuble excluding areas at a characteristic distance from the poles at early time points (marked by ch in the first panel of each sequence in Figure 4). Note that fibrils labeled with anti-TPX labeled start to accumulate over the chromatin, where they partially condense to form a nascent pole (arrow at 280 s). Next the anti-TPX2 aggregate moves distally, and the structure evolves toward symmetrical bipolarity. Figure 4B (Supplementary Video M4_2) shows an example of bipolarization by pole splitting. The initial pole is poorly focused, which was typical for CSF monopoles. Note the pole material, which is heavily labeled with anti-TPX2, splits symmetrically in two, giving rise to a bipolar spindle. Figure 4C (Supplementary Video M4_3) shows an example where pole splitting as well as new pole assembly near chromatin occur, giving rise to a tripolar spindle. Formation of assemblies that were bipolar but not symmetric or had more than two poles was common, especially in thin squashes where poles frequently split, perhaps in response to pulling forces from the glass surface. Obtaining quantitative information on microtubule and TPX2 dynamics during bipolarization was technically difficult, but we were able to measure the rate of pole separation during bipolarization by pole splitting in favorable sequences (Figure 4D). The peak rate of pole separation was ~2 μm/min for the two pole splitting sequences in Figure 4, though most of the splitting in 4B occurred at a slower rate, perhaps due to interference from the glass surface.

As with tubulin imaging alone, onset of coherent microtubule sliding in TPX2/tubulin sequences correlated with acquisition of bipolar organization. We started to see evidence for coherent movement within the structure of tubulin speckles and anti-TPX2 fibrils and puncta at the same time, as soon as two or more distinct pole-like TPX2 aggregates were present and separated. However, bipolarizing spindles typically became disorganized before we were able to observe the transition to symmetrical bipoles with bidirectional sliding. As in sequences where tubulin alone was imaged, sliding appeared to initiate over a large region of the bipolarizing structure simultaneously. Sliding took several forms, and its directions are illustrated by chevrons in Figure 4. When a new pole formed near chromatin, sliding was observed from chromatin toward the old pole and also was associated with the new pole moving away from the chromatin (Figure 4A, 980 s; Supplementary Video M4_1). When a pole split, bidirectional sliding was observed between the separating poles (Figure 4B, 525 s; Supplementary Video M4_2). Pole splitting also seemed to induce unidirectional sliding of microtubules from the chromatin toward the splitting region, giving the visual impression that the separating poles were pulling chromatin-associated microtubules into the bipolarizing region (Figure 4C, 557 s; Supplementary Video M4_3).

Role of the Ran Pathway in Generating Overlap Microtubules and Flux

Imaging of bipolarizing spindles (Figure 4) and literature models (Karsenti and Nedelec, 2004) suggested a central role for the Ran pathway in generating antiparallel microtubules that are required for bipolarization and flux. To test this, we sought to inhibit the pathway. The chromatin pathway is primarily driven by GTP exchange on Ran at chromatin, followed by release of microtubule nucleating and stabilizing factors from sequestration by importin (Gruss *et al.*, 2001; Nachury *et al.*, 2001). To inhibit this pathway, we added excess importin-alpha, an approach developed by Gruss *et al.* (2001) to inhibit microtubules nucleation driven by Ran.GTP. This protein is the NLS-binding subunit of importin (Gorlich *et al.*, 1994), and adding it in excess pushes the steady state of the Ran/importin system back toward sequestration of Ran-activated spindle components. This treatment has the advantage that it can act before or after spindle assembly and that it presumably inhibits all spindle assembly factors that are sequestered by importin. Addition of excess importin-alpha (1 mg/ml) before spindle assembly (spontaneous bipolarization or cycled spindles) blocked spindle formation, with only a few disorganized microtubules present around chromatin (unpublished data). This demonstrates the importance of the Ran/importin pathway in *Xenopus* extract spindle assembly, as previously shown (reviewed in Karsenti and Vernos, 2001). We then investigated the consequence of adding excess importin-alpha to preformed spindles, choosing the cycled spindle system so we could look at kinetochore microtubule behavior in addition to bipolarity and flux. Addition of importin-alpha (1 mg/ml) resulted in a dramatic decrease in microtubule density throughout the spindle, but spindle-shaped structures

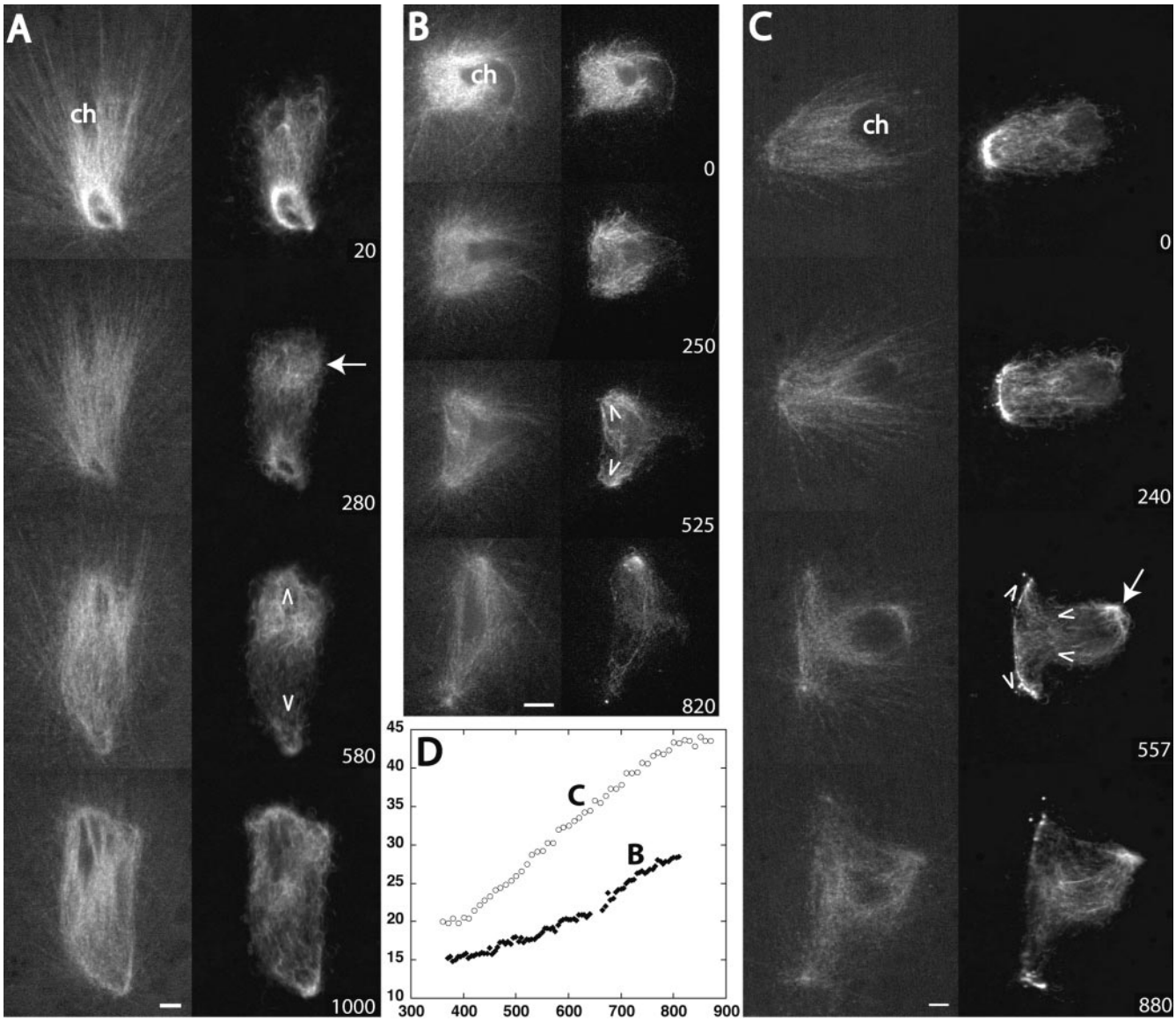

Figure 4. Pathways for spontaneous bipolarization. CSF monopoles labeled with rhodamine tubulin at speckle levels (left panels in each pair) and Alexa 488 anti-TPX2 (right panels) were imaged by spinning disk confocal microscopy. The numbers are elapsed time in seconds. The position of chromatin at the beginning of each sequence is marked ch. The direction of microtubule sliding within each structure is marked with chevrons. Bars, 5 μm. (A) Example of new pole assembly near chromatin. A cloud of fibrils labeled with anti-TPX2 forms around chromatin, marked by the arrow at 280 s. This cloud partially condenses and begins to move upward, associated with microtubule sliding (top chevron at 580 s). At the same time the lower pole becomes more focused, and sliding toward this pole initiates (lower chevron). By 1000 s the structure has evolved into an almost symmetrical bipole. See Supplementary Video M4_1. (B) Example of pole splitting. The initially unfocussed pole starts to split around 250 s. By 525 s microtubule sliding is evident, tracking with the splitting poles. See Supplementary Video M4_2. (C) Example where both pathways occur. The pole starts to split around 240 s. By 550 s the poles are separating rapidly, associated with bidirectional microtubule sliding. Around this time, a new pole coalesces near chromatin (arrow). Apparently unidirectional sliding is also microtubule sliding evident around the chromatin, transporting microtubules toward the splitting poles. By 880 s the structure has evolved into a tripolar spindle. See Supplementary Video M4_3. (D) Tracking of pole separation from the sequences in B and C. *X*-axis is time in seconds; *Y*-axis is pole-pole distance in micrometers. Average and (peak) rates of separation were ~1 (2) μm/min in B and ~2 (2.5) μm/min in C.

persisted for ~30 min. We imaged these live by confocal microscopy, adding as probes labeled tubulin at speckle levels, nonperturbing IgG to CenpA to visualize kinetochores (Maddox *et al.*, 2003) and nonpeturbing IgG to the pole protein NUMA to visualize spindle poles (Figure 5). The NUMA IgG probe was made and evaluated as described for the TPX2 IgG probe. Importin-alpha treated spindles consist largely of microtubule bundles stretching between paired sister kinetochores and poles, with very few remaining overlap microtubules (Figure 5, A and B). The lack of chromatin-associated and overlap microtubules is most evident in the supplementary videos, such as Supplementary Video M5_1. In some time-lapse sequences these reduced spindles were stable (Supplementary Video 5_1); in others they slowly collapsed (Supplementary Video M5_2). Visual inspection, and kymography, of time-lapse sequences

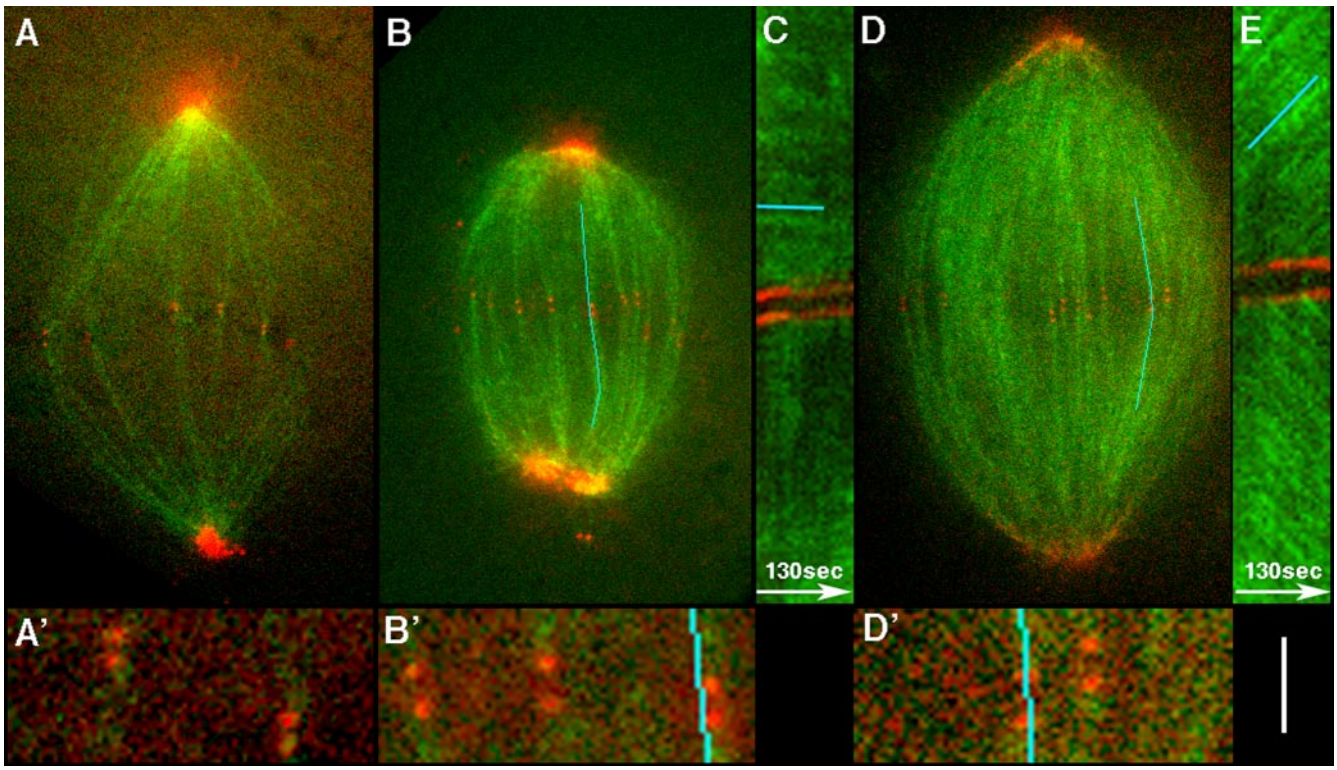

Figure 5. Removal of overlap microtubules and inhibition of flux, by excess importin-alpha. (A) Example of a spindle after addition of importin-alpha (1 mg/ml) to cycled spindles, visualized by confocal microscopy. Green is X-rhodamine-tubulin at speckle levels; red is a mixture of Alexa 488–labeled, nonperturbing IgGs to CenpA and NUMA, to visualize both kinetochores and poles. Note that prominent microtubule bundles still connect sister kinetochores to the poles. The total microtubule density is greatly reduced compared with control spindles, and overlap bundles that are prominent in control spindles are missing. A′ is a 4× magnification of the kinetochore region. See Supplementary Video M5_1. (B) Another example of an importin-alpha–treated spindle. The blue line is the center of a 7-pixel-wide line that included the kinetochore pair throughout the sequence that was used to measure the kymograph in C. B′ is a 4× magnification of kinetochore region. See Supplementary Video M5_2. (C) Kymograph from the importin-alpha–treated spindle shown in B. Note the horizontal green streaks (highlighted by blue line), indicating lack of microtubule sliding relative to the kinetochores. (D) Control spindle containing the same probes as A and B. The line is the center of a 7-pixel-wide lines that was used to measure the kymograph in E. D′ is a 4× magnification of kinetochore region. See Supplementary Video M5_3. (E) Kymograph from the control spindle shown in D. Note the diagonal green streaks, indicating microtubule sliding away from kinetochores, characteristic of poleward flux. Bar, 10 μm (A, B, and D); 2.5 μm (A′, B′, and D′); 3.3 μm (C and E).

using labeled tubulin at speckle levels revealed no evidence for microtubule sliding in the residual kinetochore fibers, implying poleward flux is completely blocked (Figure 5C, Supplementary Video M5_2). Nine importin-alpha–treated spindles were inspected for evidence of microtubule sliding. In 7 the pole-pole distance was approximately constant; in two some collapse was evident. In every case tubulin speckles appeared to be nonmoving by both visual inspection and kymography. All control spindles inspected using these methods and probes show evidence for robust, coherent, poleward movement of speckles (Figure 5E, Supplementary Video M5_3). Although sister kinetochores were still oriented toward the pole correctly in importin-alpha treated spindles, we noticed that the interkinetochore distance in sister pairs was significantly reduced, indicating reduced poleward force on kinetochores (Table 1). Interestingly, the mean distance between sisters in importin-alpha–treated spindles was significantly larger than that in nocodazole-treated spindles reported in a previous study, though the distance in control spindles was the same (Table 1). We believe that poleward force on kinetochores in metaphase *Xenopus* extract spindles is generated in part by the flux engine dragging microtubules out of kinetochores against molecular friction (Maddox *et al.*, 2003), so the reduced interkinetochore distance in importin-alpha–treated spindles is consistent with lack of flux leading to reduced poleward force. The fact that the interkinetochore distance does not fall to its fully relaxed, nocodazole length suggests some other force producing mechanism can generate poleward force on metaphase kinetochores when flux stops, such as pac-man activity (Maddox *et al.*, 2003).

Electron Microscopy of Overlap Microtubules

Our observations suggest an important role for antiparallel, overlapping microtubules for bipolarization and flux. We used electron microscopy (EM) to better characterize these microtubules in cycled spindles, where morphology and dynamics are relatively uniform. We know from confocal speckle imaging that all overlap bundles near the equator display robust, bidirectional sliding, implying they contain antiparallel microtubules (Maddox *et al.*, 2003). Spindles were diluted, fixed, sedimented, embedded, and cut into thin sections parallel to, and across, the spindle axis. In longtitudinal sections, prominent overlap bundles were observed near the metaphase plate that did not connect to kinetochores (Figure 6, A–C). In cross sections near the metaphase plate, microtubules were close together in these bundles, in many case separated by less than a microtubule

Table 1. Interkinetochore distance in sister pairs

Treatment	Mean interkinetochore distance (μm)	SD	Sample size (kinetochore pairs; spindles)
Importin-alpha[a]	0.96	0.2	67; 6
Control[a]	1.46	0.25	118; 12
Nocodazole[b]	0.6	0.4	26; nr
Control[b]	1.5	0.1	20; nr

Distance between sister kinetochores in importin-alpha– and nocodazole-treated metaphase spindles. nr, not reported.

[a] This study.

[b] From Maddox *et al.* (2003).

diameter (Figure 6, D and E). There was no obvious fixed geometry to the bundles. Rather, the bundled, overlapping microtubules appeared to be embedded in amorphous material of unknown composition that bridged nearby microtubules (Figure 6E). Dark dots were frequently associated with spindle microtubules (Figure 6, B and C). These dots are probably ribosomes in most cases. They had the same size and morphology as ribosomes decorating rough ER that was often present at the spindle pole (unpublished data). Furthermore, *Xenopus* extract spindles purified by dilution and sedimentation though a glycerol cushion contained abundant 18S and 23S rRNA (Chang, Salic, and Mitchison, unpublished data), and ribosomes are known to bind to microtubules in sea urchin egg cytosol (Suprenant *et al.*, 1989). In some cases we observed strings of amorphous material containing ribosomes connecting nearby microtubules (Figure 6B, inset), suggesting this material might have some structural role.

DISCUSSION

Do Monopoles Flux?

When we tracked speckles in computationally aligned CSF monopoles, we did not observe coherent movement of speckles toward the pole, providing the structure was unambiguously monopolar (Figure 1). We conclude that CSF monopoles most likely do not flux. Using fluorescence pho-

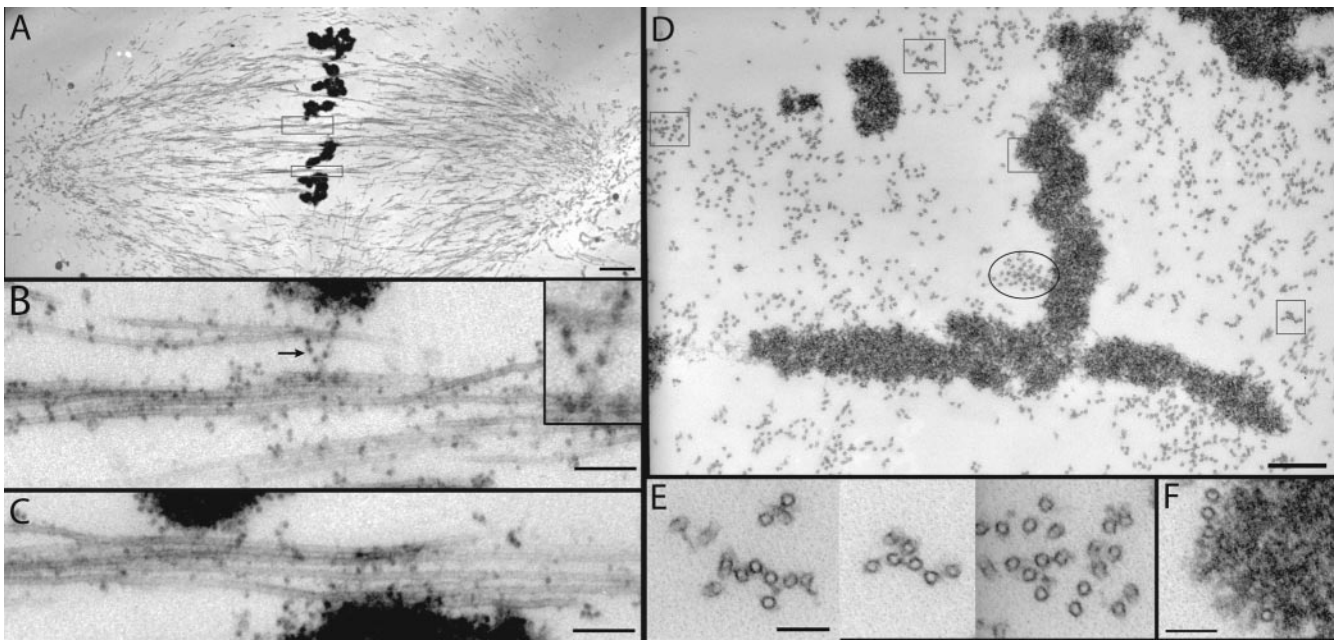

Figure 6. Electron microscopy of overlap bundles in bipolar spindles. Cycled spindles were diluted 100-fold into a microtubule-stabilizing buffer, fixed, sedimented, and sectioned as described (Ohi *et al.*, 2003). (A) Longtitudinal section through the center of a spindle. The boxed regions, containing microtubule bundles that do not attach to kinetochores, are shown magnified in B and C. (B) Longtitudinal section through a nonkinetochore bundle at the equator. We know from speckle imaging that these bundles contain antiparallel microtubules (Maddox *et al.*, 2003). Note the dark dots attached to microtubules, sometimes via amorphous material. These dots are probably ribosomes (see text). Arrow and inset show an example of a string of amorphous material containing ribosomes connecting two microtubules. (C) Another example of a nonkinetochore bundle. (D) Cross section near the equator of a different spindle. The square boxes are shown at higher magnification in E and F. The oval box marks a microtubule bundle that partly terminates in a kinetochore in adjacent sections. (E) Cross section through three nonkinetochore bundles from D. Again, mixed polarities must be present in these bundles. Note the presence of amorphous material bridging between microtubules. (F) Example of microtubules that make a lateral association with chromatin but are not part of a kinetochore fiber. Many such interactions are present. Bars (nm): A, 2000; B, 200, inset 100; C, 200; D, 500; E and F, 100.

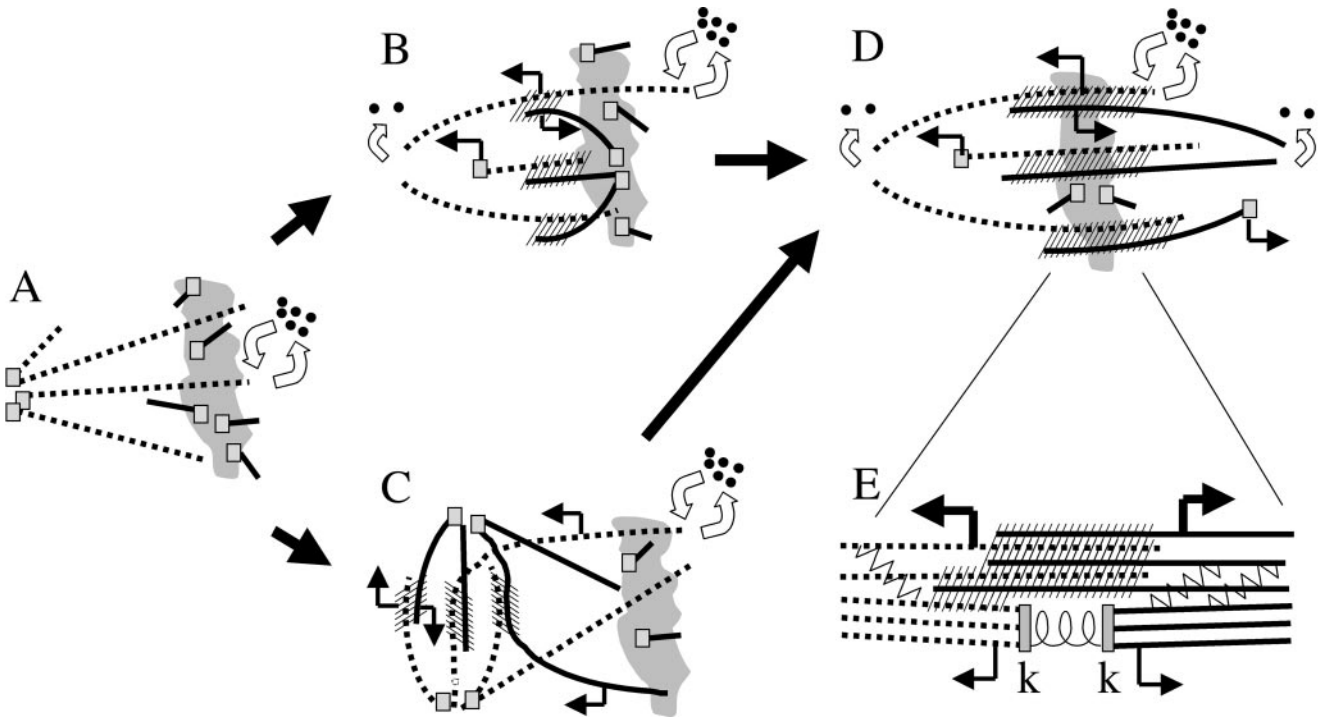

Figure 7. Models for spontaneous bipolarization. The irregular gray shape is chromatin. Dotted and solid lines are microtubules of opposite polarities. Small squares are minus end nucleating/capping complexes. Curved open arrows represent polymerization dynamics, with all plus ends undergoing dynamic instability, and uncapped minus ends undergoing slow depolymerization or some other form of instability. Straight arrows denote microtubule sliding direction. Hash marks are antiparallel interactions that generate antiparallel sliding forces, presumably through recruitment of Eg5 (Miyamoto *et al.*, unpublished results). (A) CSF Monopole. No sliding, minus ends at the pole are capped. Nucleation occurs near chromatin, to generate microtubules that are initially short and disorganized. (B) New pole assembly near chromatin. Nucleating complexes at chromatin aggregate into new pole, creating a zone of antiparallel overlap that recruits sliding motors. This tends to push the new pole outward, generating positive feedback that increases the zone of overlap, leading to bipolarization. Because the new pole moves out, minus ends at the pole must be capped. Sliding forces from the overlap zone also push microtubules toward the old pole. Because the old pole remains at approximately a constant distance from chromatin, minus ends must start depolymerizing at the old pole. How minus end dynamics are differentially regulated at the two poles is not clear. (C) Pole splitting pathway. The old pole splits, creating a zone of antiparallel overlap that recruits sliding motors. This tends to increase pole separation, generating positive feedback leading to bipolarization. Sliding apart of the poles causes microtubules near chromatin to slide toward the bipolarizing region. Minus ends must be capped at both poles during splitting, so sliding leads to pole separation rather than minus end depolymerization. (D) Steady state bipole. Nucleation continues near chromatin, and the resulting capped minus ends are moved poleward by microtubule sliding forces from overlap zones. Minus ends that reach the pole become uncapped and start to depolymerize, but note that the majority of depolymerization occurs by dynamic instability of plus ends. Nucleation, polymerization, sliding and depolymerization are balanced by unknown mechanisms to create a steady state in length and mass. (E) Hypothesis for flux in kinetochore microtubules. Anti-parallel sliding forces (heavy bent arrows) are generated in overlap bundles (hatched area), most likely by Eg5 activity. These forces are transmitted to kinetochore microtubules by cross-linking factors (zig-zag lines), and/or by kinetochore microtubules participating directly in force-generating overlap interactions (hatched area). Kinetochore microtubules respond by sliding poleward (thin bent arrows). Friction at the kinetochore resists sliding, generating poleward force that pulls sister kinetochores (k-k) apart.

toactivation to mark the lattice, Sawin and Mitchison (1994) reported sliding of microtubules to the poles in CSF monopoles and DMSO asters, though they noted that only a subset of monopoles showed evidence for flux. We believe that the conclusions of the previous study were incorrect, because it failed to take spontaneous bipolarization into account. The most important difference between this article and the previous work is the quality of the total tubulin images that were used to define whether the structure was mono- or bipolar. In the 1994 study, spontanteous bipolarization was not detected, despite our new observation that it occurred in 70% of the sequences in the kind of thin squash preparation used in the old study, and 40% of the sequences in flow chambers. Presumably spontaneous bipolarization was missed because of the extremely poor resolution afforded by imaging low levels of rhodamine tubulin with an ISIT camera. The main criterion for concluding that a CSF monopole can flux in the 1994 study was observation of unidirectional microtubules sliding. We observed that spontaneous bipolarization frequently induced microtubule sliding, which appears unidirectional if only a part of the structure is followed. For example, pole splitting induces unidirectional sliding of microtubules near chromatin toward the bipolarizing region between the separating poles (Figure 4C, Supplementary Video M4_3; see also Figure 7C). We believe that this type of sliding accounts for unidirectional movement of photoactivated bars observed in CSF monopoles in the in 1994 study. In the case of possible flux in monopolar DMSO asters, we also believe that the 1994 study was mistaken because of poor imaging of total microtubules. Using speckle imaging we have not detected coherent, poleward microtubule sliding in DMSO asters. However we have observed unpredictable splitting, fusion, and reorganization of DMSO asters in contact with glass surfaces

that might score as flux by fluorescence photoactivation if the total distribution of microtubules was poorly visualized, and we believe this accounts for the incorrect conclusion in Sawin and Mitchison (1994).

Our conclusion that monopolar asters do not flux is subject to the caveat that there is a lower bound to the rate of flux we could detect. In any fiduciary marking technique, the ability to measure microtubule lattice sliding is dependent on the relative rates of sliding and turnover. To detect sliding by speckle imaging requires that the lattice move detectably before speckles are randomized by turnover. We estimate a speckle would have to travel at least 0.5 μm during its lifetime for us to detect sliding by eye and kymograph. Turnover rate in monopolar asters has not been measured. If it occurs at the same rate as bipolar spindles ($t_{1/2} \sim$ 100 s) (Sawin and Mitchison, 1991b), then the lowest rate of flux we could detect is $\sim$ 0.3–0.6 μm/min. If turnover is faster in monopoles, the lower bound of detection would be faster. It is theoretically possible that photoactivation could detect slower flux, because it tracks only microtubules that have not turned over. However, the 1994 study reported a flux rate in CSF monopoles that was similar to bipolar spindles, so we think failure to account for spontaneous bipolarization in the 1994 study is a more likely explanation of the discrepancy. Another caveat is that speckle imaging might miss flux of a subpopulation of microtubules if that population was small and not localized. Overall, our observations rule out coherent flux in typical CSF monopoles occurring at close to the bipole rate and involving the majority of microtubules. They do not rule out slow microtubule sliding within the structure or fast sliding of some subpopulation. Improved imaging techniques would probably reveal further information on microtubule dynamics, and it would be particularly useful to develop methods for directly visualizing minus end dynamics.

Spontaneous Bipolarization

In this article we describe live observation of spontaneous bipolarization of an initially monopolar aster at a resolution high enough to track movement of speckles and TPX2 aggregates. We think these sequences provide the best description yet of this interesting process. The spontaneous bipolarization we describe is not exactly the same as physiological meiosis II spindle assembly in the *Xenopus* egg, because CSF monopoles contain a sperm centrosome at their pole, whereas physiological meiosis II occurs without centrosomes. However, our imaging did not suggest a special role for centrosomes in bipolarization, and they are known to have mainly a kinetic influence on spindle pole assembly in *Xenopus* extracts (Heald *et al.,* 1997). Thus we believe our observations are relevant to physiological meiotic spindle assembly.

Figure 7 shows models for the two spontaneous bipolarization pathways we observed. In CSF monopoles (Figure 7A) microtubules initiated from nucleating centers at the poles (squares) exhibit dynamic instability on their plus ends (double arrows) but not depolymerization of minus ends. Activation of the Ran pathway at chromatin induces microtubule nucleation there, and we hypothesize that these microtubules are initially short and disorganized. Formation of a new pole near chromatin (Figure 7B) was first evident from accumulation and aggregation of a cloud of anti-TPX2 near chromatin (Figure 4, A and C). TPX2 is released from a soluble complex with importin by Ran GTP, and Ran GTP is generated by the exchange factor RCC1 bound to chromatin (Gruss *et al.,* 2001), consistent with a central role of the Ran pathway in spontaneous bipolarization. Inhibition of factors downstream of Ran activation by addition of importin-alpha to assembled spindles resulted in depletion of overlap microtubules and cessation of flux (Figure 5), again consistent with a central role of the Ran pathway. We thus favor a model in which activation of Ran promotes both nucleation of microtubules, and their organization into antiparallel overlap bundles, shown hatched in Figure 7. These bundles play a central role in generating the forces that promote both bipolarization in the assembling spindle and the sliding force for flux at steady state. Karsenti and Nedelec (2004) have discussed similar ideas. Pole splitting (Figure 7C) was more common in thin squashes than thicker preparations and might be initiated in part by forces from dynein attached to the glass, exerting outward directed force on the pole through astral microtubules (which is not shown in figure). Once antiparallel overlaps assemble between the separating poles (hatched in Figure 7, B and C), they help push the poles apart. We hypothesize that physiological meiotic spindle assembly occurs without centrosomes by a combination of the two pathways. However, bipolarization is initiated, our observations suggest that once part of the assembly achieves antiparallel organization, the whole structure rapidly becomes bipolar, and we never observed bipolar structures reverting to monopolarity. This suggests the existence of a positive feedback loop involving antiparallel microtubule organization, bidirectional sliding, and pole splitting. Once initiated, this loop rapidly and irreversibly drives the whole assembly toward bipolarity.

Implications for Flux Mechanism in Xenopus *Extract Spindles*

Our data are consistent with a model in which antiparallel microtubule bundles assembled near chromatin in response to Ran activation are necessary for both bipolarization and concerted microtubule sliding within the meiotic spindle. What does this tell us about the molecular mechanisms underlying poleward flux? We now believe that the sliding component of poleward flux is driven by the activity of the plus end directed kinesin Eg5 (Miyamoto *et al.,* 2004). The simplest interpretation of our data is that Eg5 generates the sliding force for bipolarization and flux by cross-bridging antiparallel microtubules, as proposed previously (Mitchison and Sawin, 1990; Kashina *et al.,* 1996; Sharp *et al.,* 2000). Eg5 is enriched at poles, though it is also present in the overlap region, and its dynamics are complex (Kapoor and Mitchison, 2001). Thus Eg5 probably does more than simply driving sliding in overlap microtubules; for example, it may also help position pole complexes. The organization of overlap bundles at the EM level (Figure 6) suggests that they are not bundled by Eg5 alone. The distance between neighboring microtubules is quite variable, and microtubules appear to be embedded in an unidentified amorphous substance that also contains ribosomes. To fully understand bipolarization, flux, and the role of Eg5, it will be necessary to probe Eg5 dynamics in more detail, determine how it targets to spindle microtubules, and also to determine the biochemical composition of overlap bundles.

Figure 7 also highlights some of the many open questions in meiotic spindle assembly, notably the related questions of how minus end dynamics are regulated and how the spindle achieves a steady state in length. Minus ends are broadly distributed in steady state bipoles (Valloton *et al.,* 2003). We observed continuous transport of the pole component TPX2 from chromatin toward poles (Figure 3) and loss of overlap microtubules and flux when the Ran pathway was inhibited with excess importin-alpha (Figure 5). These data suggest that nucleation occurs continuously near chromatin at

steady state, followed by poleward transport of minus ends, as illustrated in Figure 7D. In Figure 7 we speculate that minus ends exist in two states, capped (by squares in the figure) and uncapped, to account for the fact that minus ends must be stable when new poles are moving out, or newly nucleated minus ends are transported away from the chromatin, and unstable once they reach the steady state length. This instability could be due to continuous minus end depolymerization (curved arrows in Figure 7, B and D) or inability to regrow after depolymerization from the plus end. How the transition from stable to unstable minus ends occurs and why it is apparently sensitive to both bipolarity and chromatin-pole distance is unknown. In our model, the transition from stable to unstable minus ends sets spindles length, so it will be important to elucidate its biochemical basis.

If antiparallel organization is required for microtubule sliding within the spindle, how do kinetochore fibers flux? We hypothesize that sliding force is generated in antiparallel bundles by Eg5. It is either transmitted to kinetochore fibers by cross-linking or by participation of kinetochore microtubules in force-producing, antiparallel interactions. (Figure 7E). Consistent with this hypothesis, removal of antiparallel microtubules by addition of excess importin-alpha leaves behind kinetochore microtubules that no longer flux (Figure 5). Transmission of sliding force from antiparallel to kinetochore microtubules by cross-linking and/or cobundling predicts that there could be shear between the two populations of microtubules if kinetochores imposed drag, as we think they do (Maddox *et al.*, 2003). Using kymography of speckles, Maddox *et al.* (2003) observed that kinetochore microtubules slide poleward on average ~10% slower than neighboring antiparallel bundles. This implies shear between the two populations, though it will be important to remeasure shear with more accurate speckle tracking methods (Valloton *et al.*, 2004). In extract spindles, overlap bundles are present very close to kinetochores, and the two populations of microtubule often merge into single bundles within a micrometer of kinetochores (Ohi *et al.*, 2003). Tight and local cross-linking between the two populations may account for the relatively low amount of shear between them. In mammalian somatic spindles, kinetochore fibers are thought to slide poleward at less than half the rate of overlap bundles (Waterman-Storer *et al.*, 1998). This potentially large differential in sliding rates needs to be tested by more systematic studies. If confirmed, a larger rate differential in mammalian cells could be rationalized by the fact that the ratio of kinetochore to overlap microtubules is higher and/or because the two populations are less intimately connected by cross bridges (McDonald *et al.*, 1992).

Our conclusion that poleward microtubule sliding requires antiparallel overlap cannot necessarily be extended to other types of spindle, because different spindles are known to exhibit distinct organization and dynamics. Recent evidence has shown that kinetochore fibers that are isolated from the rest of the spindle can still slide poleward in some systems (Khodjakov *et al.*, 2003; Chen and Zhang, 2004). An important question in these systems is whether the microtubules in the isolated kinetochore fibers are homopolar or if they participate in direct or indirect antiparallel interactions, as diagrammed in Figure 7E. More work is required to determine if poleward flux in different spindles results from common or distinct molecular mechanisms and if antiparallel overlap is universally required.

Meiotic spindle assembly, with its robust achievement of bipolarity, and a steady state in length, is a beautiful example of self-organization in the cytoplasm. Our experiments point to the importance of chromatin-induced microtubule nucleation and assembly of antiparallel bundles that produce sliding force, in self-organization of bipolarity. To progress in understanding this biology we need more information on the Ran pathway, the biochemistry of antiparallel overlap interactions, and how minus end dynamics are regulated.

ACKNOWLEDGMENTS

We thank members of the MBL Cell Division Group and our winter labs for discussion, K. Burbank for computational help, E. Karsenti for stimulating suggestions during manuscript revision, and K. Weis for providing the importin-alpha clone. This work was funded by National Institutes of Health grants GM39565 (T.J.M.), GM24364 and GM606780 (E.D.S.), and by MBL fellowships from UIC Inc. and Nikon Inc.

REFERENCES

Brust-Mascher, I., and Scholey, J.M. (2002). Microtubule flux and sliding in mitotic spindles of *Drosophila* embryos. Mol. Biol. Cell *13*, 3967–3975.

Chen, W., and Zhang, D. (2004). Kinetochore fibre dynamics outside the context of the spindle during anaphase. Nat. Cell Biol. *6*, 227–231.

Desai, A., Murray, A., Mitchison, T.J., and Walczak, C.E. (1999a). The use of *Xenopus* egg extracts to study mitotic spindle assembly and function in vitro. Methods Cell Biol. *61*, 385–412.

Field, C.M., Oegema, K., Zheng, Y., Mitchison, T.J., and Walczak, C.E. (1998). Purification of cytoskeletal proteins using peptide antibodies. Methods Enzymol. *298*, 525–541.

Gorlich, D., Prehn, S., Laskey, R.A., and Hartmann, E. (1994). Isolation of a protein that is essential for the first step of nuclear protein import. Cell *79*, 767–778.

Gruss, O.J. *et al.* (2001). Ran induces spindle assembly by reversing the inhibitory effect of importin alpha on TPX2 activity. Cell (2001). *104*, 83–93.

Heald, R., Tournebize, R., Blank, T., Sandaltzopoulos, R., Becker, P., Hyman, A., and Karsenti, E. (1996). Self-organization of microtubules into bipolar spindles around artificial chromosomes in *Xenopus* egg extracts. Nature *382*, 420–425.

Heald, R., Tournebize, R., Habermann, A., Karsenti, E., and Hyman, A. (1997). Spindle assembly in *Xenopus* egg extracts: respective roles of centrosomes and microtubule self-organization. J. Cell Biol. *138*, 615–628.

Kapoor, T.M., and Mitchison, T.J. (2001). Eg5 is static in bipolar spindles relative to tubulin: evidence for a static spindle matrix. J. Cell Biol. *154*, 1125–1133.

Karsenti, E., and Vernos, I. (2001). The mitotic spindle: a self-made machine. Science *294*, 543–547.

Karsenti, E., and Nedelec, F. (2004). The mitotic spindle and actin tails. Biol. Cell *96*, 237–240.

Kashina, A.S., Baskin, R.J., Cole, D.G., Wedaman, K.P., Saxton, W.M., and Scholey, J.M. (1996). A bipolar kinesin. Nature *379*, 270–272.

Khodjakov, A., Cole, R.W., Oakley, B.R., and Rieder, C.L. (2000). Centrosome-independent mitotic spindle formation in vertebrates. Curr. Biol. *10*, 59–67.

Khodjakov, A., Copenagle, L., Gordon, M.B., Compton, D.A., and Kapoor, T.M. (2003). Minus-end capture of preformed kinetochore fibers contributes to spindle morphogenesis. J. Cell Biol. *160*, 671–683.

Kirschner, M., and Mitchison, T. (1986). Beyond self-assembly: from microtubules to morphogenesis. Cell *45*, 329–342.

Maddox, P.S., Bloom, K.S., and Salmon, E.D. (2000). The polarity and dynamics of microtubule assembly in the budding yeast *Saccharomyces cerevisiae*. Nat. Cell Biol. *2*, 36–41.

Maddox, P., Desai, A., Oegema, K., Mitchison, T.J., and Salmon, E.D. (2002). Poleward microtubule flux is a major component of spindle dynamics and anaphase a in mitotic *Drosophila* embryos. Curr. Biol. *12*, 1670–1674.

Maddox, P., Straight, A., Coughlin, P., Mitchison, T.J., and Salmon, E.D. (2003). Direct observation of microtubule dynamics at kinetochores in *Xenopus* extract spindles: implications for spindle mechanics. J. Cell Biol. *162*, 377–382.

Mallavarapu, A., Sawin, K., and Mitchison, T. (1999). A switch in microtubule dynamics at the onset of anaphase B in the mitotic spindle of *Schizosaccharomyces pombe*. Curr. Biol. *9*, 1423–1426.

Matthies, H.J., McDonald, H.B., Goldstein, L.S., and Theurkauf, W.E. (1996). Anastral meiotic spindle morphogenesis: role of the non-claret disjunctional kinesin-like protein. J. Cell Biol. *134*, 455–464.

McDonald, K.L., O'Toole, E.T., Mastronarde, D.N., and McIntosh, J.R. (1992). Kinetochore microtubules in PTK cells. J. Cell Biol. *118*, 369–383.

Mitchison, T., Evans, L., Schulze, E., and Kirschner, M. (1986). Sites of microtubule assembly and disassembly in the mitotic spindle. Cell *45*, 515–527.

Mitchison, T.J., and Sawin, K.E. (1990). Tubulin flux in the mitotic spindle: where does it come from, where is it going? Cell Motil. Cytoskelet. *16*, 93–98.

Miyamoto, D.T., Perlman, Z.E., Burbank, K.S., Groen, A.C., and Mitchison, T.J. (2004). The kinesin Eg5 drives poleward microtubule flux in Xenopus extract spindles. J. Cell Biol. (*in press*).

Nachury, M.V., Maresca, T.J., Salmon, W.C., Waterman-Storer, C.M., Heald, R., and Weis, K. (2001). Importin beta is a mitotic target of the small GTPase Ran in spindle assembly. Cell *104*, 95–106.

Nedelec, F. (2002). Computer simulations reveal motor properties generating stable antiparallel microtubule interactions. J. Cell Biol. *158*, 1005–1015.

Ohi, R., Coughlin, M.L., Lane, W.S., and Mitchison, T.J. (2003). An inner centromere protein that stimulates the microtubule depolymerizing activity of a KinI kinesin. Dev. Cell (2003). *5*(2), 309–321.

Rebollo, E., Llamazares, S., Reina, J., and Gonzalez, C. (2004). Contribution of noncentrosomal microtubules to spindle assembly in *Drosophila* spermatocytes. *2*, 54–64.

Rogers, G.C., Rogers, S.L., Schwimmer, T.A., Ems-McClung, S.C., Walczak, C.E., Vale, R.D., Scholey, J.M., and Sharp, D.J. (2004). Two mitotic kinesins cooperate to drive sister chromatid separation during anaphase. Nature *427*, 364–370.

Mitchison, T.J., and Sawin, K.E. (1990). Tubulin flux in the mitotic spindle: where does it come from, where is it going? Cell Motil. Cytoskelet. *16*(2), 93–98.

Sawin, K.E., and Mitchison, T.J. (1991a). Mitotic spindle assembly by two different pathways in vitro. J. Cell Biol. *112*, 925–940.

Sawin, K.E., and Mitchison, T.J. (1991b). Poleward microtubule flux mitotic spindles assembled in vitro. J. Cell Biol. *112*, 941–954.

Sawin, K.E., and Mitchison, T.J. (1994). Microtubule flux in mitosis is independent of chromosomes, centrosomes, and antiparallel microtubules. Mol. Biol. Cell *5*, 217–226.

Sharp, D.J., Rogers, G.C., and Scholey, J.M. (2000). Microtubule motors in mitosis. Nature *407*, 41–47.

Smirnova, E.A., and Bajer, A.S. (1998). Early stages of spindle formation and independence of chromosome and microtubule cycles in *Haemanthus* endosperm. Cell Motil. Cytoskelet. *40*, 22–37.

Suprenant, K.A., Tempero, L.B., and Hammer, L.E. (1989). Association of ribosomes with in vitro assembled microtubules. Cell Motil. Cytoskelet. *14*, 401–415.

Vallotton, P., Ponti, A., Waterman-Storer, C.M., Salmon, E.D., and Danuser, G. (2003). Recovery, visualization, and analysis of actin and tubulin polymer flow in live cells: a fluorescent speckle microscopy study. Biophys. J. *85*, 1289–1306.

Walczak, C.E., Vernos, I., Mitchison, T.J., Karsenti, E., and Heald, R. (1988). A model for the proposed roles of different microtubule-based motor proteins in establishing spindle bipolarity. Curr. Biol. *8*, 903–913.

Waterman-Storer, C.M., Desai, A., Bulinski, J.C., and Salmon, E.D. (1998). Fluorescent speckle microscopy, a method to visualize the dynamics of protein assemblies in living cells. Curr. Biol. *8*, 1227–1230.

Wittmann, T., Wilm, M., Karsenti, E., and Vernos, I. (2000). TPX2, a novel *Xenopus* MAP involved in spindle pole organization. J. Cell Biol. *149*, 1405–1418.